Using Symbolic Analysis of Local Field Potentials for Anesthesia Depth Prediction

Ioana Onofrei
Computer Science
Technical University of Cluj-Napoca
Cluj-Napoca, Romania
ioana.onofrei01@gmail.com

Andreea Sălăgean
Computer Science
Technical University of Cluj-Napoca
Cluj-Napoca, Romania
andreea.salagean@yahoo.com

Narcisa Sîrca
Computer Science
Technical University of Cluj-Napoca
Cluj-Napoca, Romania
narcisa.teodora16@gmail.com

Vasile V. Moca
Transylvanian Institute of Neuroscience
Cluj-Napoca, Romania
moca@tins.ro

Adriana Nagy-Dăbâcan
Transylvanian Institute of Neuroscience
Cluj-Napoca, Romania
dabacan@tins.ro

Raul C. Mureșan
Transylvanian Institute of Neuroscience
Cluj-Napoca, Romania
muresan@tins.ro

Rodica Potolea
Computer Science
Technical University of Cluj-Napoca
Cluj-Napoca, Romania
rodica.potolea@cs.utcluj.ro

Mihaela Dinșoreanu
Computer Science
Technical University of Cluj-Napoca
Cluj-Napoca, Romania
mihaela.dinsoreanu@cs.utcluj.ro

Camelia Lemnaru
Computer Science
Technical University of Cluj-Napoca
Cluj-Napoca, Romania
camelia.lemnaru@cs.utcluj.ro

***Abstract*—Depth of anesthesia (DOA) is a very important parameter, determining how the brain responds to various concentrations of anesthetic. Here, we assess the dependence of DOA on the concentration of isoflurane by analyzing local-field potentials (LFPs) recorded in mouse visual cortex. To capture the DOA-related changes, we employed TESPAR and Fourier-based feature extraction techniques, combined with machine learning. In addition, we performed an analysis of bursts present in LFP signals and evaluated their influence on DOA classification. These bursts are characterized by high amplitudes and low frequencies, requiring different analysis approaches: one that removes the high amplitudes and the other one that filters the lower frequencies. We developed procedures that successfully discriminate between different levels of anesthesia. Our study indicates a correlation between increased isoflurane dose and LFP amplitude suppression and also indicates that large amplitude bursts are expressed in the signal in a dose-dependent manner.**

***Index Terms*—LFP, anesthesia, burst, TESPAR, FFT, mice, ML**

I. Introduction

Interventions under general anesthesia are important in medical practice, but they are also widespread in research fields, such as neuroscience, where animal models are often used. In all cases, it is crucial to maintain depth of anesthesia (DOA) at an appropriate level. Too deep anesthesia and patients can suffer permanent damage or even risk death. This is why it is preferable to err on the lighter side of the DOA. On the other hand, a too light anesthesia leads to unwanted awareness and associated psychological trauma [1], especially when neuromuscular blockade is involved [2]. A review has shown that the reported cases of unwanted awareness is highly variable, ranging from 1 in 20000 to as high as 1 in 600 cases [3]. Similarly, for acute neuroscience experiments under anesthesia, if DOA is too light the animal might be suffering, which is unethical and, in many cases, can ruin the outcome of the experiment. On the other hand, too deep anesthesia has a tremendous impact on the nervous system whose activity can be silenced to the point recorded data shows no useful feature. In both cases, experimental results can be compromised by inadequate anesthesia.

Despite the importance and incontestable benefits of anesthetics in medical care, their mechanisms of action are not well understood. For instance, it has been suspected for a long time that they act on the neurons' cell membrane. However, for volatile anesthetics, such as isoflurane, the action mechanism was only recently revealed [4]. Added to these unknowns are the interindividual variability and the large number of available anesthetic cocktails used in practice, making anesthesia research considerably harder. This depicts an active and lively research field, which considers that the main *modus operandi* of anesthetics is to disconnect local networks from the nervous system. In this way, although the painful stimulus is processed by primary sensory systems, it does not reach consciousness [5]. Indeed, it has been shown that anesthetic action is reflected by the brain's electrical activity, such as the electroencephalogram (EEG) and LFPs, which has allowed the creation of automated EEG-DOA monitors for medical applications [6]. These EEG monitors rely on time and spectral features, on entropy and complexity measures, and on symbolic analysis while taking into account the well known burst suppression phenomenon [6] [7]. While looking for DOA correlates in neural signals, similar methods of investigations as for EEG

were also employed in LFP studies [8].

Given the incidence and critical consequences of unwanted awareness, there is clearly room for improvements in DOA assessment. We aim to investigate the impact of the anesthetics on the electrical brain activity. In this respect we need to identify the signal features that are sensitive to the DOA related changes. To address these issues, we conducted a study on local field potentials (LFP) recorded from mice. We first analyzed how LFPs change with different concentrations of isoflurane anesthesia. Next, we used machine learning to discriminate between three DOA levels: deep, medium, light and we interpreted the classification results based on the observed changes in the LFP. To discriminate and classify the three DOA levels, we used signal features that comprise both time and frequency domain characteristics namely: the Time Encoded Signal Processing And Recognition (TESPAR) symbolic analysis [9] and the well-known Fast Fourier Transform (FFT).

II. Materials and methods

A. Electrophysiology

LFPs are electrophysiology signals recorded intracranially, with a frequency range up to 300 Hz. They reflect electrical potentials distributed across a wider neuronal population in the vicinity of the recording electrode, as well as afferent synaptic inputs [10]. LFP data was recorded from mouse primary visual cortex using a Multichannel Systems amplifier fitted with a 32 electrode Neuronexus probe type A4x2-tet. The probe consists of four shanks, each shank disposing of two tetrodes (with four contacts each). Compared to single-shank probes, this configuration offers the possibility to sample a larger cortical surface (tangentially) [11]. Data from two animals, which will be referred to further as M014 and M013, was recorded using the same experimental protocol.

Animal experiments were carried out respecting directive 86/609/EEC of the European Communities Council from 24 November 1986, directives 2010/63/EU of the European Parliament and 2010/63/EU of the Council from 22 September 2019, and according to the guidelines of the Society for Neuroscience, Romanian laws for the protection of animals, and Romanian law 206/2004 on good conduct in scientific research. Experiments were approved by the local ethics committee (approval 3/CE/02.11.2018) and by the National Sanitary-Veterinary (approval ANSVSA 147/04.12.2018). The number of animals used was kept to a minimum.

B. Experimental protocol

The current work relies on data from experiments designed to study visual response of the mouse brain under the influence of three DOA levels. Anesthesia was controlled by adjusting the concentration of Isoflurane anesthetic through a vaporizer device connected to an oxygen tank [11].The mouse inhaled the gas mixture via a tailored mask. The three DOA levels correspond to precise Isoflurane concentrations: 2% for deep, 1.75% for medium and 1.5% for light anesthesia. The external simulation plays an important part in DOA assessment [6]. Here, the experimental protocol employed visual simulation in the form of moving gratings displayed on a screen placed in front of the animal. The gratings combined one of each: four different orientations, eight moving directions, and three possible visual contrasts resulting in a set of 240 trials, each corresponding to the display of a particular moving grating (Fig. 1). The images shown to the animal were precisely controlled and synchronized with the recorded neuronal activity.

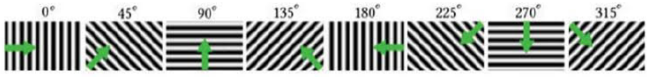

Fig. 1: The eight grating orientations used during the experiments [11]

Each stimulus presentation was packed in a trial with a well determined succession of events: Trial start, Stimulus ON, Stimulus OFF and Trial End (see Fig. 2). Here we focused on two segments of the trial namely spontaneous (from Trial Start to Stimulus ON) and stimulus (between Stim ON and Stim OFF), with reference to the nature of the activity recorded in that segment. Each recording electrode, or channel, was studied separately, as each registered the electrical potentials in its proximity. The full set of trials was repeated for each depth of anesthesia, meaning that we had at least a set of 240 trials for each DOA recorded by all 32 electrodes. We say at least, because trial sets were run several times for the same depth of anesthesia [11]. We first analyzed the dataset and optimized the methods on one of the mice, and then we applied the same for the second mouse to see to what extent, the approach can be generalized.

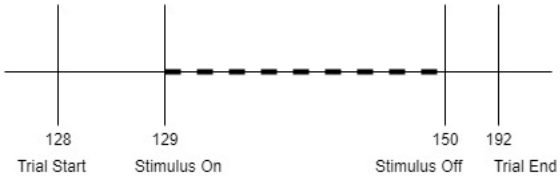

Fig. 2: Trial structure. Event codes and their meanings are shown under the timeline.

C. Preprocessing

The data was recorded at a frequency of 32kHz and afterwards downsampled at 1kHz. Following the recording, two Butterworth IIR filters of 3rd order were applied: a low-pass filter at 300Hz and a high-pass at 0.1Hz and the DC-component was removed. We kept the preprocessing to a minimum during this research project, on top of the previous standard procedures, the frequency space of interest was filtered using two Butterworth IIR filters: a high-pass filter of order 5 at 1Hz and a low-pass 3rd order at 150Hz. In addition, the line noise was removed with the help of a band stop 5th order filter with cut-off frequencies at 49 and 51Hz.

D. Bursts of low frequency and high amplitude

Preliminary analyses showed that the neural signal presents regions with atypical behavior characterized by large amplitudes and seemingly low frequencies that stood out from the rest of the signal. These periods are called bursts. In order to determine the effects of the bursts on the analyses we performed, we first needed to detect them. To this end we used interquartile range (IQR) to determine the amplitude thresholds that can identify bursts in the signal. By rejecting the burst periods, we obtained two different datasets: first, the initial dataset, only with preprocessing and the second dataset with bursts removed.

Furthermore, spectral analysis using FFT revealed that most of the signal's power was concentrated in the low frequencies below 10Hz. Besides, a high standard deviation appeared between the trials of the same channel. This made us wonder if bursts had any contribution to this high power in the lower frequencies. To test this hypothesis, we applied a new additional filter, a 3rd order Butterworth High-Pass filter with cutoff frequency at 10Hz. We obtained thus, the third dataset.

E. Features extraction

We were interested in feature extraction methods able to capture most of the DOA relevant features of the LFP signal. Thus, we focused on two methods: FFT and TESPAR, which will be detailed below. From each trial, we extracted the features from both 'spontaneous' and 'stimulus' trial segments.

With FFT we aimed to explore common patterns found in various frequency ranges. To this end, with the Welch periodogram we quantified the average LFP power in the following seven biological-relevant frequency bands: delta (1.5-4 Hz) , theta (4-8 Hz), alpha (8-12 Hz), beta (12- 30Hz), gamma low (30- 50 Hz), gamma high (50-80 Hz), and fast (80-130 Hz). Seven average power values were obtained for one trial corresponding to each of the above-mentioned frequency bands. These frequency bands are well established in the neuroscience literature and pertain to oscillations' different roles, emergence mechanisms, and cognitive correlates [12] [7].

By contrast, TESPAR operates in the time domain and is suitable for capturing the time-varying characteristics of the signal, revealing changes in the properties of the signal's source – the brain. By comparison to FFT, it hides small details and therefore it is robust to noise and can reveal information that is not distinguishable in the frequency-domain [13].

The basic concept of TESPAR [9] is to represent the signal as a set of epochs defined as the signal periods between two consecutive zero crossing points. Each such epoch is then associated with two descriptors:

- D - "the duration", referring to the number of samples
- S - "the shape", representing the number of local minima

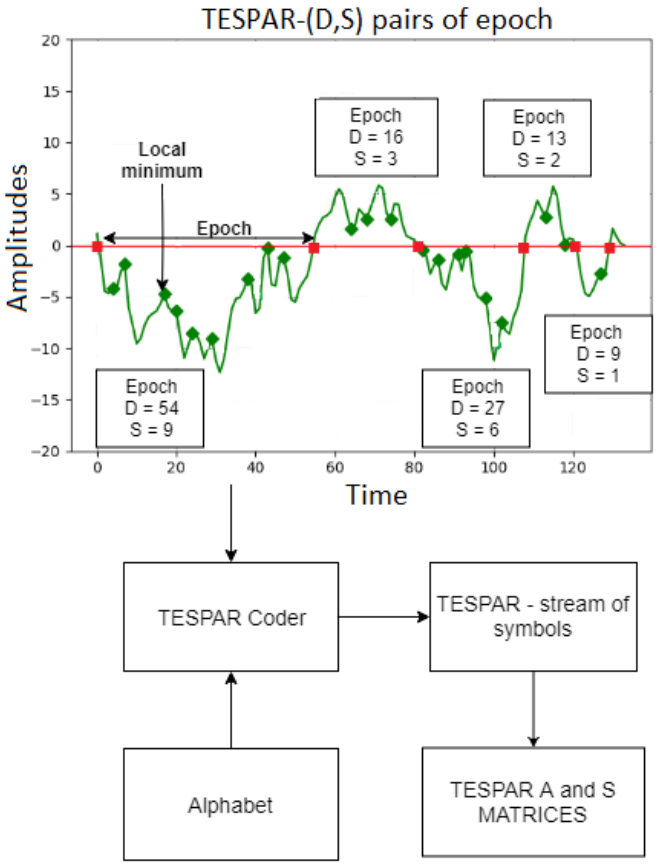

Fig. 3: TESPAR method process

Having the signal epochs coded into two-dimension vectors (D-S pairs), TESPAR uses an alphabet to assign each pair to a symbol. Here we used a vector quantization algorithm, namely Linde-Buzo-Gray [14], in order to map the distribution of epochs in the DS space and to create a codebook of 32 symbols [13]. The symbols are ordered according to the D and S dimensions of the epochs, therefore symbols with small identifier numbers (ID) correspond to short epochs with higher frequencies, while higher ID symbols correspond to long epochs with lower frequencies. The codebook maps similar epochs to the same symbol, which in turn renders the method robust to small variations and noise (3). Next, the signal transformed into a stream of symbols is organized into two fixed sized descriptors (Fig. 3), which can easily be fed into classification algorithms:

- *S matrix* - one-dimension vector that counts the number of occurrences for each symbol (Fig 4).
- *A matrix* - two-dimensional matrix, that contains the number of symbols pairs that appear l symbols apart. Where l is the "lag" parameter through which the temporal information is incorporated. We chose a small value for l, being interested in the short time evolution of the signal (Fig 5).

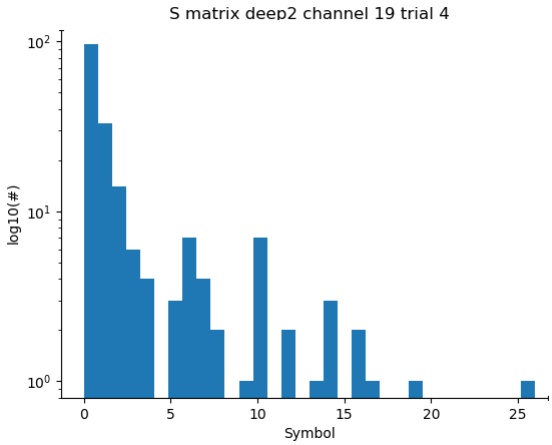

Fig. 4: Example of a TESPAR S matrix for one trial and one channel

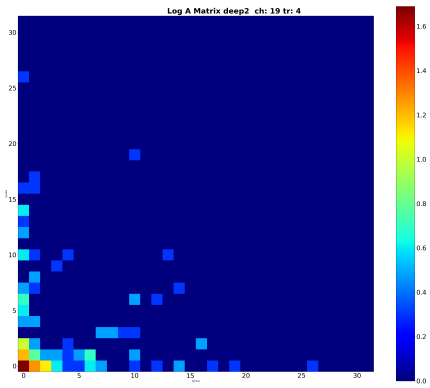

Fig. 5: Example of a TESPAR A matrix for one trial and one channel.

It is worth underlying that both the Welch periodogram and TESPAR map the signal into fixed size descriptors, regardless of its length. This has many advantages for both statistics and classification algorithms.

F. Classifiers

While an important part was to understand what are the LFP properties that are changed by isoflurane, another major target of the current research was to discriminate between three DOA levels. To this end, we employ machine learning algorithms well suited for classification of labeled data [15]. Here we used three supervised classifiers that are different in terms of properties and approach. The classifiers capture different aspects of the data with the hope that additional information can be gained by comparing the classification performance between algorithms. The hyperparameters of each were selected using a grid search technique.

Our first choice of classifier, given the brain is a highly non-linear system, was the Support Vector Machine (SVM) [16]. SVM is effective in high dimensional space and versatile due to the possible usage of different kernel functions. When fed with FFT descriptors, the selected kernel was of "linear" type and C=1000; while for TESPAR A matrix or combinations of the two kind of features, the selected kernel was "rbf", gamma="auto" and C=1.0. By contrast, our second choice, the Decision Trees, are linear classifiers that offer very good data adaptability, and are easy to interpret and use [17]. The model uses "gini" criterion for splitting and the tree's maximum depth is of two. In addition, to these two we also employed the Random Forest classifier, which is robust, flexible and offers greater accuracy due to its collection of prediction trees [18]. The classifier was configured with the following parameters: "max_depth= 5", "n_estimators= 5000", "min_samples_leaf"= 5, "min_samples_split= 10".

G. Evaluation

Because DOA classes are of equal importance and data is balanced, the appropriate metric for evaluation the performance of ML algorithms is the accuracy score. Each classification was performed repeatedly 20 times. In each iteration the dataset was split into train and test subsets, in proportion of 80% and 20% respectively. The train data, known as "seen" data, were used to instruct the model. The remaining "unseen" data, belonging to the test set, were further used to measure the predictability performance of the model. This iteration is equivalent to a round of cross-validation, 20 repetitions providing a good variability of the test subset. The final result consised in the mean value and the standard deviation of the individual scores obtained for each of the splits.

III. Results

A. Bursts analysis

Preliminary analyses(see II.D) showed bursts of very high amplitudes and low frequencies in the LFP. We sought to first determine their properties with respect to the DOA level. Indeed, we found a negative correlation between the administered isoflurane concentration and duration of bursty region relative to trial length, Tab. I.

We further considered the following burst characteristics: signal power, region length spanned by the burst, and the number of burst regions that occurred within a trial. These properties were also modulated by the isoflurane concentration, Tab. I. Namely, the burst regions are shorter, less frequent but having higher amplitudes with increased anesthesia.

TABLE I: Properties of burst. M014 dataset

DOA	1. Percent of burst in a trial	2. Power of burst signal	3. Nr. of burst regions in a trial	4. Duration of a burst region [ms]
light 1	51.9%	781.05	1.53	1573.45
light 4	32.4%	779.73	1.57	857.88
medium 3	25.3%	871.79	1.31	753.95
medium 5	21.2%	719.43	1.16	618.61
deep 2	16.5%	1640.96	0.86	536.02

The analysis suggests that bursts are anesthesia-dependent and may contain relevant information for DOA classification. Importantly, the same behavior was visible when we examined the second dataset, M013 (results not shown).

B. Slow trends

During preliminary analyses using the Fourier Transform, we observed slow changes in the properties of cortical responses that seemed to be caused by changes in the cortical state. Following up on this observation, we looked into how the average power within the biologically relevant bands (see above) changed in time. We found that the signal was dominated by a gradual, descending drift according to the order in which the trial-sets were recorded (Fig. 6a). We believe the explanation for this constant trend is that the brain is adapting to anesthesia through a homeostatic process.

It is worth mentioning that this trend could be caused also by factors related to the experiment itself (i.e. electrode movement, tissue damage, differences between channel impedances/signal amplitudes etc.). To eliminate this hypothesis, we performed a Z-score normalization over the channels and repeated the analyses. Even if inter-channel variability was no longer present, a descending drift in time was maintained between the power bands belonging to trial-sets with equivalent dose of isoflurane (Fig. 6b).

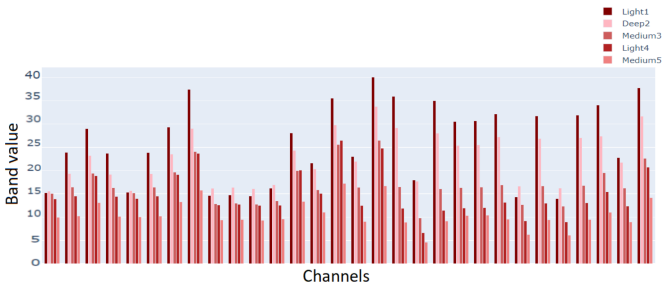

(a)

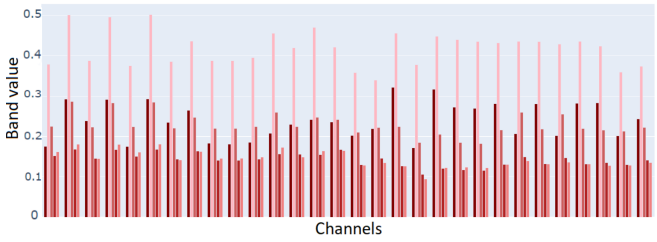

(b)

Fig. 6: Delta power band comparison between channels - the descending trend dominating anesthesia levels. (a): initial bands values. (b): bands values after Z-score normalization:

Concluding, although the experiments were recorded with equal concentration of anesthetic, the power of the signal spectrum decreased the longer the mouse was kept under anesthesia. The same trends were observed in the second mouse.

C. Particular behavior of the channels

Due to several factors, the activity recorded on individual electrodes has different characteristics. For instance, the electrode impedance, determines the amplitude range of the recorded signals, which renders direct comparison between channel power pointless and also affects FFT-based classification. In order to mitigate this issue, the Z-Scoring normalization was used. Fig. 7 demonstrates the balancing of the average power bands between channels, before and after the transformation.

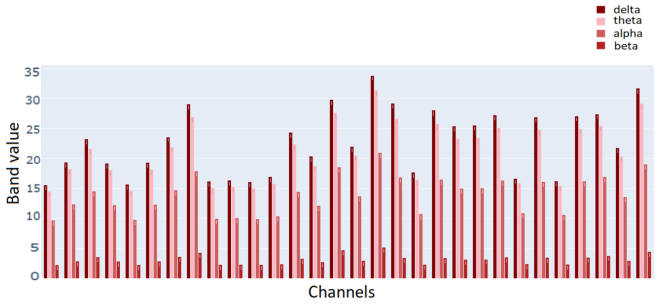

(a)

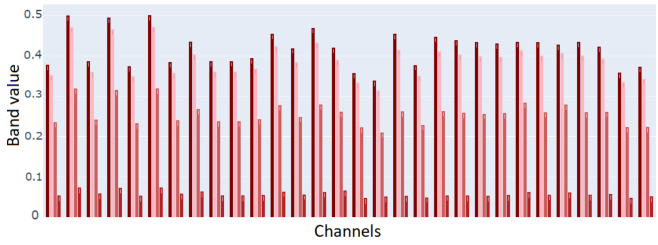

(b)

Fig. 7: Average power bands comparison between channels - deep level of anesthesia. (a): initial bands values. (b): bands values after Z-score normalization

However, other factors associated with the experiment(see III.B), also greatly impact the individual characteristics of data on each of the channels. We therefore expect that some channels will have activity that is superior in capturing the DOA-related changes as compared to other. The classification performance is illustrated in the following section.

D. Classification

We display the accuracy scores and the standard deviations obtained for all three classifiers. In cases where parts of the trials were removed due to burst some of the trials had to be rejected. In these cases, we used balanced subsets from each class by reducing the number of trials to the minimum number of trials left in a class.

The results are shown in a conjunction between a classifier: Decision Trees (DT), Random Forest (RF), Support Vector Machine (SVM), and the features configuration: A TESPAR matrix, FFT descriptors or a combination of them. We selected three channels (9, 19, 32) out of the total of 30, that we considered to be representative for the process to illustrate the changes that intervened, if any.

In order to trace the effect of the bursting regions on the classification process, we conducted the classification on the 3 conditions of the dataset mentioned in II-D. The following three tables, Tab. II, III and IV, present some of the best outcomes of the **binary** classification of deep and light DOAs, using data from M014.We depict the selected features and channels on the rows and the mean accuracy score (acc) and its standard deviation (std) for 20 runs, for each algorithm, on the columns.

TABLE II: Accuracy score of binary classification obtained for classic state of dataset

L1D2 M014 classic		DT		RF		SVM	
Features	Channel	**acc.**	std.	**acc.**	std.	**acc.**	std.
TESPAR A matrix	9	79.27	3.24	81.45	5.09	**85.26**	3.99
	19	75.62	3.06	91.14	2.34	**88.85**	2.53
	32	75.00	3.39	84.37	6.02	**85.05**	3.81
FFT descriptors	9	**87.29**	2.70	**93.02**	1.74	79.32	3.29
	19	**94.58**	1.60	**95.59**	0.98	78.48	3.68
	32	**88.54**	4.00	**92.91**	2.45	80.93	2.42
TESPAR A matrix and FFT	9	86.87	4.63	86.45	3.51	84.42	3.33
	19	94.37	2.76	92.70	2.83	88.17	1.92
	32	89.06	3.76	87.5	2.23	83.59	3.56

TABLE III: Accuracy score of binary classification obtained for remove_burst of dataset, consisting in 93 trials per class

L1D2 M014 no burst		DT		RF		SVM	
Features	Channel	**acc.**	std.	**acc.**	std.	**acc.**	std.
TESPAR A matrix	9	69.75	9.74	70.50	2.83	81.44	5.22
	19	71.00	6.61	72.96	4.26	86.49	4.27
	32	69.19	12.02	68.59	5.75	81.71	6.19
FFT descriptors	9	**92.30**	2.27	93.30	1.75	**88.40**	5.09
	19	**96.16**	2.35	99.05	0.62	**95.66**	4.67
	32	**92.89**	2.62	95.97	0.82	**93.17**	3.61
TESPAR A matrix and FFT	9	90.87	1.84	**99.69**	0.90	82.07	7.44
	19	95.66	2.53	**99.62**	1.11	86.46	7.19
	32	88.60	5.95	**99.40**	1.19	81.73	6.95

TABLE IV: Accuracy score of binary classification obtained for the dataset fitered with a High-Pass filter of 10 Hz

L1D2 M014 HP 10		DT		RF		SVM	
Features	Channel	**acc.**	std.	**acc.**	std.	**acc.**	std.
TESPAR A matrix	9	88.02	3.87	91.66	2.71	95.05	1.88
	19	86.97	3.30	91.66	1.61	96.45	1.78
	32	**90.20**	3.84	90.20	2.09	94.27	2.36
FFT descriptors	9	87.50	3.32	90.10	1.81	94.11	1.72
	19	**96.87**	1.23	95.52	1.61	**97.29**	1.52
	32	88.85	2.18	**91.35**	2.67	93.59	1.75
TESPAR A matrix and FFT	9	**90.20**	2.60	**93.12**	1.98	**95.46**	2.51
	19	94.37	1.55	**95.93**	1.50	96.25	2.24
	32	88.12	2.09	90.52	1.64	**94.37**	2.38

1) Classic: In table II we show the accuracy score of all 3 algorithms for the classic preprocessing condition of the dataset. The results reach the highest values for FFT descriptors and when these are combined with the TESPAR A matrix. On the other hand, the SVM model performs best when fed TESPAR A matrix, due to its good adaptation to multi-dimensional feature space.

2) Remove Bursts: In table III we can see the accuracy score of all 3 algorithms for the 'remove burst' condition of the dataset. As already mentioned, when it comes to this condition, some of the trials are fully discarded and for the remaining trials, we omit the bursting signal in the feature extraction process, leading to a reduced input space, of 93 trials per class. Considering that the spectrum is sensitive to oscillations, by removing the bursts, the outliers are removed, and the FFT descriptors are no longer dominated by them, consequently their relevance for DOA increases. As shown in the table, all the models discriminated the DOAs well when fed with FFT descriptors, even though they 'saw' a smaller number of training samples due to missing trials. For RF, excellent performance was obtained when combining the features.

Comparing the values in Tab. II and III, the conclusion is that TESPAR descriptors are affected by the burst removal and that is reflected in the classification performance of all three models.

3) Filtered with high-pass 10: Very good results were obtained when the whole dataset was filtered with the Butterworth High-Pass filter of 10 Hz, being less important if the features are TESPAR, FFT, or their combination. We can see the results in Tab. IV; the accuracy score is improved in comparison with the score obtained for "classic" condition, Tab. II, for each ML algorithm and for each feature configuration. This improvement is due to the fact that the frequency bands that presented the highest deviation were filtered out. A great performance indicator is also the reduced standard deviation of accuracy score exhibited.

4) Results on second animal: Reproducing the same experiments on data from M013 (results not shown), led to similar results and the same conclusions regarding the contribution of the burst regions for the classification.

5) 3 classes classification: In Tab. V we show the outcome of the multinomial classification, involving all the deep, medium and light DOAs, on data from M014. We noticed that light DOA is easiest to learn, while medium DOA is often confused with both 'deep' and light anesthesia.

TABLE V: Accuracy 2 classes L1D2M3 M014 filtered with High-Pass 10 Hz

L1D2M3 M014 HP 10		DT		RF		SVM	
Features	Channel	**acc.**	std.	**acc.**	std.	**acc.**	std.
TESPAR A matrix	9	55.97	3.48	65.00	2.36	**70.86**	3.29
	19	55.34	2.52	66.38	3.37	67.74	1.90
	32	59.37	3.53	61.73	2.02	**68.75**	2.60
FFT descriptors	9	**73.33**	3.28	**80.48**	2.56	65.13	4.00
	19	**75.20**	3.15	**83.81**	3.41	**73.50**	2.82
	32	**68.54**	3.05	**79.86**	3.59	66.45	3.69
TESPAR A matrix and FFT	9	72.84	2.88	67.15	2.19	69.27	3.37
	19	75.20	3.47	70.62	2.93	68.88	3.02
	32	69.30	2.95	65.5	2.56	66.56	4.34

IV. Discussion

Here we have investigated the effect of isoflurane anesthesia on the LFP in primary visual cortex of anesthetized mice during a visual stimulation paradigm. Our purpose was twofold: first, to investigate the changes induced by isoflurane in the activity of the visual cortex, and second, to determine, with the help of machine learning, whether DOA information can

be recovered from the LFP. Given that the same concentration of anesthetic is known to have effects of different strengths depending on the individual subject [19], our study can provide the grounds for a methodology aimed at achieving individually fine-tuned anesthesia useful for acute electrophysiology experiments and beyond.

One striking feature of the data are the bursts of low frequency and high amplitudes that we observed in the data. One of our first questions was on the nature of these bursts. They bear a strong resemblance to cortical avalanches [20] that occur naturally in anesthetized rats [21] and awake monkeys [22] and are correlated with increased spiking activity and synchrony [22]. Like avalanches, the bursts we observe occur spontaneously and are not aligned to the trial structure of the experiments, but instead they depend on the administered isoflurane concentration. The number of bursts and their length decreases with increased anesthetic concentration, while, at the same time, their amplitude increases. One possibility is that a compensation mechanism tries to make up for reduced bursts occurrence by increasing amplitude as part of some homeostatic process.

Outside bursts, high concentration of isoflurane suppresses the LFP, whose amplitude drops to levels comparable to high frequency noise-like activity. This is clearly visible in both the power spectra and in the TESPAR matrices where short symbols (higher frequencies) increase at the detriment of long ones (short frequencies). To summarize, with increased anesthesia two strong effects were observed: i) bursts increase in amplitude and power but are shorter and less frequent, while ii) outside bursts, activity drops to noise level, as expected [6]. These have contradictory effects in the power spectrum which renders separation of DOA states not so straightforward.

Similarly, high amplitude bursts and quenched LFP periods were also observed in the cortex and thalamus of rats under isoflurane [8] and is similar to the burst suppression phenomenon (BS). BS is known to be induced by trauma and anesthetics such as isoflurane [23], being characterized by bursts of activity intermixed with periods of silence [19]. It is quite possible that the bursts of activity we observe are a sign of avalanches in the light sedation states, while they reflect BS in deep anesthesia, explaining their different characteristics. In another study [24] it was shown that isoflurane BS occurs for concentrations between 2-3.5%, which supports the above view of transition from avalanches to BS.

Oddly enough, BS is considered to be a state of hypersensitivity to external stimuli [24] [23], followed by a post-burst refractory period. This would imply that visual stimulation imposes some sort of timing on the bursts. However we observe no such relation. Nevertheless, the mechanisms behind BS are not well understood [24] and other factors might be involved in generating the activity we observe in V1 as suggested by the classifications.

Clearly, classifications show that isoflurane influences the cortical responses in V1 outside bursty regions. Machine learning algorithms can distinguish quite well between the low and high doses of isoflurane, even if burst periods are completely ignored. However, the bursts and BS are a strong effect, one that can be used constructively to quantify the DOA. Indeed, keeping the bursts or at least their frequency components above 10Hz is beneficial for the classification of DOA states.

Another interesting observation is that the effect of anesthetics has a slow time component. That is, the overall activity seems to decrease with the time the animal is kept under anesthesia, the same isoflurane concentration producing quantitatively different responses depending on the cortical state. This falls in line with the well-known variability of responses to anesthetics [19]. Given this inter and intra-individual variability of responses, it is important to detect a state of "proper anesthesia" for which burst and burst-suppression can be extremely helpful.

V. Conclusion

Finally, we want to emphasize that this study uses visual stimulation to asses DOA. While stimulus usage for DOA evaluation is not new, most studies use auditory evoked potentials [19] [1] and, much less, visual evoked potentials [25]. Even fewer studies employ visual stimulations without evoked potentials. Our study shows that the effects of anesthesia on visual responses are strong enough to detect DOA-related changes even without bursts and BS. This has direct implication for the interpretation of acute experiments in visual cortex under general anesthesia.

Acknowledgment

This work was supported by a grant from the Romanian National Authority for Scientific Research and Innovation CNCS-UEFISCDI (project number COFUND-NEURON-NMDAR-PSY) and one National Science Foundation grant (number NSF-IOS-1656830) funded by the US Government.

References

[1] S. Pockett, "Anesthesia and the electrophysiology of auditory consciousness," *Consciousness and cognition*, vol. 8, pp. 45–61, 04 1999.

[2] S. Tasbihgou, M. Vogels, and A. Absalom, "Accidental awareness during general anaesthesia - a narrative review," *Anaesthesia*, vol. 73, pp. 112–122, 01 2018.

[3] J. Pandit, J. Andrade, D. Bogod, J. Hitchman, W. Jonker, N. Lucas, J. Mackay, A. Nimmo, K. O'Connor, E. O'Sullivan, R. Paul, J. Palmer, F. Plaat, J. Radcliffe, M. Sury, H. Torevell, M. Wang, J. Hainsworth, and T. Cook, "5th national audit project (nap5) on accidental awareness during general anaesthesia: summary of main findings and risk factors†‡," *British journal of anaesthesia*, vol. 113, 09 2014.

[4] M. Arif, N. Petersen, H. Wang, R. Lerner, and S. Hansen, "Studies on the mechanism of general anesthesia," *Proceedings of the National Academy of Sciences*, vol. 117, p. 202004259, 05 2020.

[5] M. Alkire, A. Hudetz, and G. Tononi, "Reviews consciousness and anesthesia," *Science (New York, N.Y.)*, vol. 322, pp. 876–80, 12 2008.

[6] V. Moca, B. Scheller, R. Mureşan, M. Daunderer, and G. Pipa, "Eeg under anesthesia–feature extraction with tespar," *Computer methods and programs in biomedicine*, vol. 95, pp. 191–202, 04 2009.

[7] B. Musizza and S. Ribaric, "Monitoring the depth of anaesthesia," *Sensors (Basel, Switzerland)*, vol. 10, pp. 10 896–935, 12 2010.

[8] A. Silva, H. Cardoso-Cruz, F. Silva, V. Galhardo, and L. Antunes, "Comparison of anesthetic depth indexes based on thalamocortical local field potentials in rats," *Anesthesiology*, vol. 112, p. 355–363, 2010.

[9] R. King and T. Phipps, "Shannon, tespar and approximation strategies," *Computers & Security*, vol. 18, pp. 445–453, 12 1999.

[10] A. Destexhe and C. Bedard, "Local field potential," *Scholarpedia*, vol. 8, no. 8, p. 10713, 2013, revision #137113.
[11] A. Dabacan, "Cellular membrane properties - effect on neural network dynamics," Ph.D. dissertation, Technical University of Cluj Napoca, 2016.
[12] M. Penttonen and G. Buzsáki, "Natural logarithmic relationship between brain oscillators," *Thalamus Related Systems*, vol. 2, pp. 145–152, 04 2003.
[13] Moca, E. Lupu, and P. Pop, "Tespar coding method evaluation in speaker recognition experiments," 05 2005.
[14] Y. Linde, A. Buzo, and R. Gray, "An algorithm for vector quantizer design," *IEEE Transactions on Communications*, vol. 28, no. 1, pp. 84–95, 1980.
[15] M. Pal, "Random forest classifier for remote sensing classification," *International Journal of Remote Sensing*, vol. 26, no. 1, p. 217–222, 2005.
[16] C. Cortes and V. Vapnik, "Support-vector networks," *Machine learning*, vol. 20, no. 3, pp. 273–297, 1995.
[17] S. R. Safavian and D. Landgrebe, "A survey of decision tree classifier methodology," *IEEE Transactions on Systems, Man, and Cybernetics*, vol. 21, no. 3, pp. 660–674, 1991.
[18] L. Breiman, "Random forests," *Machine Learning*, vol. 45, no. 1, pp. 5–32, Oct 2001.
[19] I. J. Rampil, "A primer for eeg signal processing in anesthesia," *Anesthesiology*, vol. 89, p. 980–1002, 1998.
[20] J. M. Beggs and D. Plenz, "Neuronal avalanches in neocortical circuits," *The Journal of Neuroscience*, vol. 23, p. 11167–11177, 2003.
[21] E. D. Gireesh and D. Plenz, "Neuronal avalanches organize as nested theta- and beta/gamma-oscillations during development of cortical layer 2/3," *Proceedings of the National Academy of Sciences*, vol. 105, p. 7576–7581, 2008.
[22] T. Petermann, T. C. Thiagarajan, M. A. Lebedev, M. A. L. Nicolelis, D. R. Chialvo, and D. Plenz, "Spontaneous cortical activity in awake monkeys composed of neuronal avalanches," *Proceedings of the National Academy of Sciences*, vol. 106, p. 15921–15926, 2009.
[23] J. D. Kenny, M. B. Westover, S. Ching, E. N. Brown, and K. Solt, "Propofol and sevoflurane induce distinct burst suppression patterns in rats," *Frontiers in Systems Neuroscience*, vol. 8, 2014.
[24] D. Kroeger and F. Amzica, "Hypersensitivity of the anesthesia-induced comatose brain," *Journal of Neuroscience*, vol. 27, p. 10597–10607, 2007.
[25] R. S and S. Mv, "Intraoperative visual evoked potentials: There is more to it than meets the eye," *Journal of Neurology and Neuroscience*, vol. 7, 2016.